# Ponderful

PONDS FOR CLIMATE

# Deliverable D3.1

## Protocol for Remote Sensing (RS)

## Mapping Pondscapes

Pond Ecosystems for Resilient Future Landscapes in a Changing Climate

This project has received funding from the European Union's Horizon 2020 Research and Innovation Programme under Grant Agreement No ID 869296

Ponderful Partners:


**University of Vic – Central University of Catalonia** (Spain) – Prof. Sandra Brucet (PI, Project coordinator), Dr. Diana van Gent (Project Manager)

**IGB im Forschungsverbund Berlin (Germany)** – Dr. Thomas Mehner (PI, Task lead 2.4)

**Katholieke Universiteit Leuven (Belgium)** – Dr. Luc De Meester (PI, WP2 coordinator)

**Haute Ecole Spécialisée de Súisse occidentale (Switzerland)** – Dr. Beat Oertli (PI, WP4 coordinator)

**Universitat de Girona (Spain)** –Dr. Dani Boix (PI)

**Ecologic Institut gemeinnützige GmbH (Germany)** – Dr. Manuel Lago (PI, Task lead 1.4)

**University College London (UK)** –Dr. Carl Sayer (PI)

**Middle East Technical University (Turkey)**– Dr. Meryem Beklioğlu (PI)

**CIIMAR - Interdisciplinary Centre of Marine and Environmental Research (Portugal)** –Dr. José Teixeira (PI, WP5 co-coordinator)

**Aarhus University (Denmark)** – Dr. Thomas A. Davidson (PI)

**Uppsala University (Switzerland)** –Dr. Malgorzata Blicharska (PI)

**Bangor University (UK)** – Dr. Isabel Rosa (PI)

**Technical University of Munich (Germany)** – Dr. Johannes Sauer (PI, Task lead 1.6)

**I.S.A.R.A. – Institut Supérieur d'Agriculture Rhône-Alpes (France)** – Dr. Joël Robin (PI)

**Middle East Technical University (Turkey)** – Dr. Meryem Beklioğlu (PI)

**Freshwater Habitats Trust (UK)** – Dr. Jeremy Biggs (PI, WP5 co-coordinator)

**Universidad de la República (Uruguay)** – Dr. Matías Arim (PI)

**Randbee Consultants SL (Spain)** – Juan Arevalo Torres (PI)

**Amphi International APS (Denmark)** – Lars Briggs (PI, Task lead 5.4)

# Ponderful

**Authors:**
Zuhal Akyurek, Çağrı Karaman

**Contributors:**
Isabel Rosa, Dennis Trolle, Matías Arim, Sandra Brucet

**Document title:** Deliverable D3.1 – Remote Sensing (RS) Mapping Protocol
**Document Type:** Deliverable

**WP No:** 3
**WP Title:** Scenarios and Modelling
**WP Lead:** BU

**Date:** 31 May 2021
**Document Status:** Final version

This project has received funding from the European Union's Horizon 2020 Research and Innovation Programme under Grant Agreement No ID869296

# Table of contents

# Executive Summary

The Protocol for Remote Sensing for Mapping Ponds will be used for mapping the ponds that will be sampled in WP2 and ponds in 8 DEMO-sites chosen in Europe and Uruguay in WP4. This protocol presents the use of optical satellite images having medium spatial resolution (10-20 m) in mapping the ponds. Linear spectral unmixing and k-means unsupervised classification algorithms are used to map the ponds. The ponds having surface area greater than 0.5 ha can be mapped with the methodology presented in this protocol. For the ponds smaller than 0.5 ha,mapping accuracy changes with respect to the month and/or land use around the ponds. In wet season and having less green vegetation around the ponds, the identification accuracy of the ponds from Sentinel 2A images is high.

# Introduction

The Protocol for Remote Sensing for Mapping Ponds will be used for mapping the ponds that will be sampled in WP2 and ponds in 8 DEMO-sites chosen in Europe and Uruguay in WP4. This protocol will be applied in 2021 and 2022 on all ponds and pondscapes. It constitutes the deliverable D3.1 (delivering date: May 2021).

The protocol describes how spatio-temporal distribution of pondscapes is mapped using available remote sensing data, with a focus on assessing hydroperiods (the period in which a soil area is waterlogged) of the ponds where the stratified sampling will be organized and of DEMO-site ponds. The protocol describes the methods to pre-process remote sensing data, algorithm of pond detection, temporal changes (hydroperiod) and validation methods.

The output will be a user-friendly web application, which will present the spatial and temporal distribution of the ponds retrieved from satellite data, GIS shape files or raster layers with location and attributes of identified ponds.

# Methods

## 3.1. Remote Sensing in mapping water surfaces

Remote sensing technology offers effective ways to observe surface water dynamics. Remote sensing data sets provide spatially explicit and temporally frequent observational data of a number of physical attributes about the Earth's surface that can be appropriately leveraged to map the extent of water bodies at regional or even global scale, and to monitor their dynamics at regular and frequent time intervals. There are generally two categories of sensors that can serve the purpose of measuring surface water—the optical sensor and the microwave sensor. Microwave sensors, due to their usage of long wavelength radiation, have the ability to penetrate cloud coverage and certain vegetation coverage. Independent of solar radiation, they can work day and night under any weather condition. Optical sensors have been widely applied in this field due to high data availability, as well as suitable spatial and temporal resolutions (Huang et al., 2015). Huang et al. (2018) present a review of using remote sensing in mapping water areas on the Earth surface and state that the number of publications has increased steadily after 2000.

Landsat imagery is the most popular data source for calculating water indices, due to its suitable spectral bands, as well as its medium spatial resolution. The Landsat program is the longest-running enterprise for acquisition of satellite imagery of Earth. Starting from 1972, the program has been running and the instruments on the Landsat satellites have acquired millions of images. The Sentinel missions include radar and super-spectral imaging for land, ocean and atmospheric monitoring. Each Sentinel mission is based on a constellation of two satellites to fulfill and revisit the coverage requirements for each mission, providing robust datasets for all Copernicus services. Missions started in 2014 and since then Sentinel satellites have acquired images that were used in ocean and atmospheric monitoring. Comparison of Landsat 7 and 8 bands with Sentinel-2 is given in Figure 1.

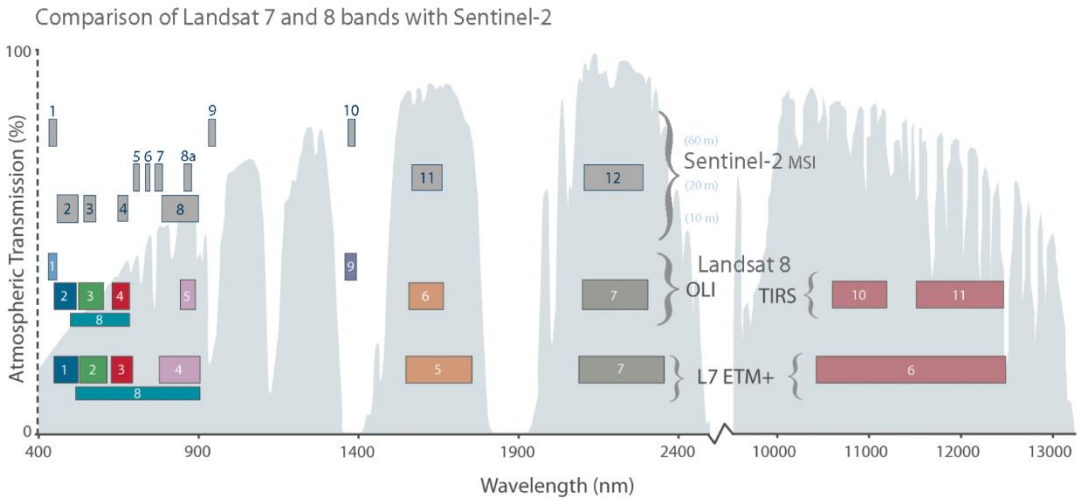


Figure 1 Comparison of Landsat 7 and 8 bands with Sentinel-2

The principle of extracting surface water from optical images is obviously lower reflectance of water, compared to that of other land cover types, in infrared channels. Many methods have been developed for extracting water areas from optical remote sensing imagery (Frazier & Page, 2000; Manavalan et al., 1993; Ozesmi & Bauer, 2002; Acharya et al., 2016; Olthof, 2017; Sun et al., 2011). An easy and effective way to identify water is to use water indices, which are calculated from two or more bands, to identify the differences between water and non-water areas. Many indices have been developed to identify surface water areas, such as normalized difference water index (NDWI; McFeeters, 1996), and modified NDWI (mNDWI; Xu, 2006). McFeeters's NDWI can be regarded as the first generation of water index. It was widely used in the first 10 years of the 21st century (Chowdary et al., 2008; Hui et al., 2008). Later, Xu (2006) found that the Short-wave Infrared (SWIR) band is able to reflect some subtle characteristics of water, and so replaced the Near Infrared (NIR) band in NDWI with the SWIR band and proposed the mNDWI. It is now widely accepted that mNDWI is more stable and reliable than NDWI, because the SWIR band is less sensitive to concentrations of sediments and other optical active constituents within the water than the NIR band (Figure 2). Therefore, mNDWI has been widely used in many recent studies (Chen et al., 2014; Mohammadi et al., 2017). One limitation of mNDWI is that it cannot discriminate between water and snow, because although the snow has a generally higher reflectance than the water in all the visible and infrared channels (Figure 2), the normalized difference between Green band and SWIR band for snow is as high as that of water. Therefore, many studies (e.g., Choi & Bindschadler, 2004; Salomonson & Appel, 2004) used the normalized difference snow index (NDSI), which has an identical formula to mNDWI, to extract snow cover. The timeline of development of major water indices and launch of satellite/sensors is given in Figure 3.

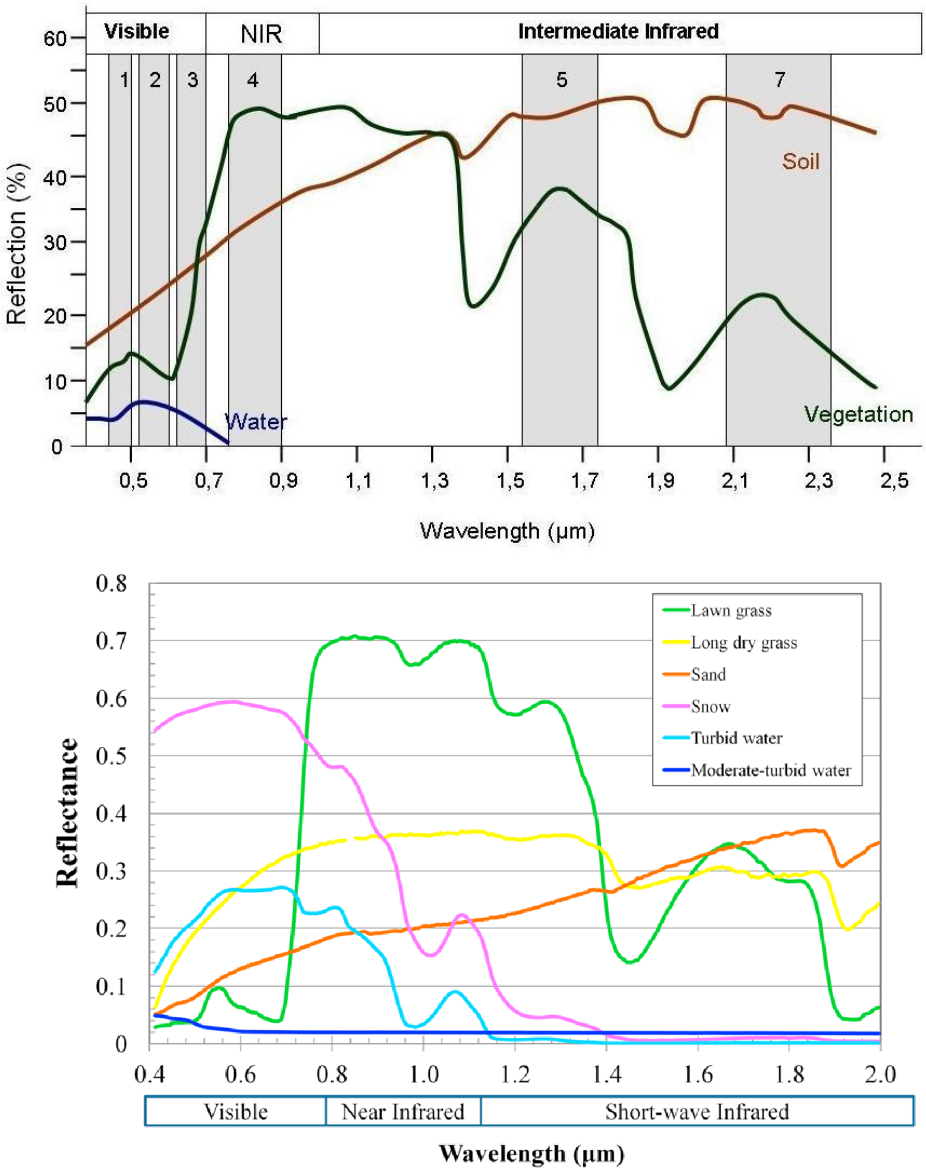


Figure 2 Reflectance of water, soil and vegetation (a), Reflectance of several typical land cover objects, collected from United States Geological Survey (USGS) digital spectral library (https://speclab.cr.usgs.gov/spectral-lib.html)

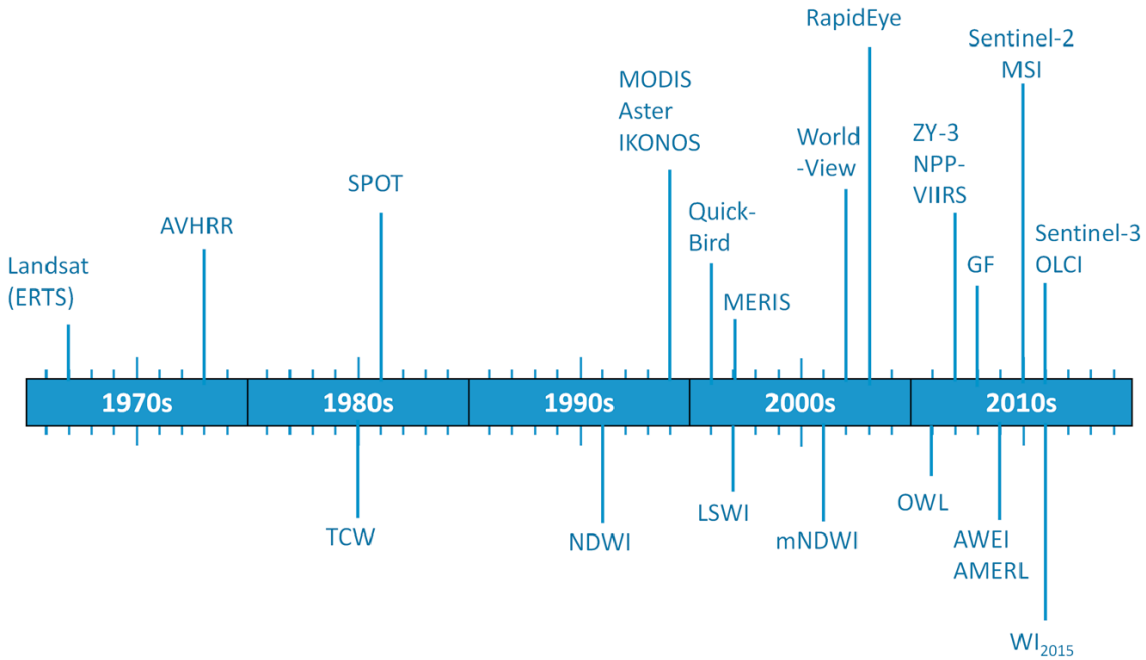


Figure 3 Timeline diagram of development of major water indices and launch of satellites/sensors (Huang et al., 2018).

3.2. Mapping ponds and pondscapes

i-Data used and web-application development

Ponds (small standing waters varying in size from 1 m2 to about 2-5 ha in area that may be permanent or seasonal, man-made or naturally created) are crucial for biodiversity conservation, supporting a larger proportion of rare, endemic and threatened freshwater species than lakes or rivers, and are key elements of blue landscape connectivity. Mapping ponds from satellite images has several limitations. The optical sensors vary significantly in their applicability, based largely on their spatial, temporal, spectral, and radiometric resolutions. Temporal and spatial resolutions determine the scale of processes that can be captured by a given sensor. In general, land surface sensors have a finer spatial resolution (~10–30m) but coarser temporal resolution (~1–2 weeks), allowing them to detect spatial patterns in water quality in smaller water bodies (e.g., small lakes and rivers) but with only 1–2 observations per month depending on the sensor and cloud cover conditions (Topp et al., 2020).

The Copernicus Sentinel-2, wide-swath, high-resolution, multi-spectral imaging mission is used to monitor water bodies in mapping the ponds. Mission aims monitoring variability in land surface conditions with 290 km swath width and up to 10 days revisit time. Sentinel 2 Level-2A product can be utilized since it provides Bottom of Atmosphere (BOA) reflectance images. Its spatial and temporal resolution are much better than the available satellite images having medium size spatial resolution. Sentinel-2A satellite was launched on 23 June 2015 and has been in operation over 5 years.

Landsat 8 was developed as a collaboration between NASA and the U.S. Geological Survey (USGS) and launched on February 11, 2013. It aims to monitor the Earth and to keep track of changes on the planet's surface from the impact of both nature and humans. Mission provides continuity with the more than 40-year long Landsat land imaging data set. The satellite consists of two science instruments—the Operational Land Imager (OLI) and the Thermal Infrared Sensor (TIRS). These two

sensors provide seasonal coverage of the global landmass at a spatial resolution of 30 meters (visible, NIR, SWIR); 100 meters (thermal); and 15 meters (panchromatic). The Landsat 8 scene size is 185-km-cross-track-by-180-km-along-track with revisit time of 16 day.

Pond locations (GPS coordinates) retrieved from local databases are used as ground truthing data. The selected ponds in WP2 and WP4 are collected in a database. Geocoded and detailed GIS layers showing all small water bodies in national databases of Switzerland, Turkey and Spain are already obtained. Geospatial attributes of small water bodies such as area, perimeter, elevation are calculated and used as ground truth. The ponds of the other countries will be obtained and stored in the same database which will be deliverable (Spatial database shared; D3.3). An example of the database is given in Appendix 1.

The Google Earth Engine (GEE) has been used as a platform since it provides cloud-based geospatial processing platform to store and process satellite imagery. The current archive of data includes those from other satellites, as well as Geographic Information Systems (GIS) based vector data sets, social, demographic, weather, digital elevation models, and climate data layers. Moreover, GEE offers Application Programming Interface (API) that allows interaction with Python client libraries.

ii- Pond detection algorithm

The most direct approach towards extracting surface water is to classify the remotely sensed image and count the number of pixels per class over the region of interest. This can be achieved by extracting information from an image using classification algorithms. Each pixel represents a series of measurements in several spectral bands of the reflectance from a particular ground area. Pixels having similar spectral behavior forms spectral classes. By assigning each pixel to a spectral class that resembles most, a classification of the entire image is obtained.

Classification strategies can be grouped into two categories as supervised and unsupervised classification and often combined into hybrid methodologies using more than one method (Richards, 2013). Unsupervised image classification is a method in which the algorithm separates a large number of unknown pixels in an image based on their reflectance values into classes or clusters with no direction from the analyst (Tso & Mather, 2010). One of the more common methods based on this principle is K-means clustering (MacQueen, 1967). Although this procedure requires virtually no human intervention and is based purely on spectrally pixel-based statistics, the analyst must supply a mapping between the spectral and the informational classes afterwards.

Supervised classification, on the other hand, demands much more interaction with the analyst. Analyst defines small areas called training sites on the image that are known to represent certain informational classes. These training areas should be homogenous enough to represent spectral properties of land cover class. In the subsequent classification stage, all pixels are assigned to the informational (sub)classes they resemble most. An example of supervised classification is maximum likelihood classification.

Considerable number of mixed pixels are present in every remotely sensed image. This occurs where objects are relatively small compared to the spatial resolution of the scanner and results in errors in classification. (Gebbinck, M. S., 1998) (Figure 4).

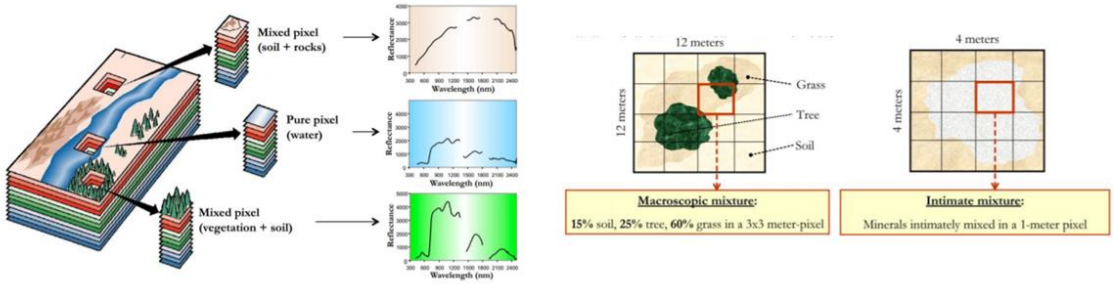


Figure 4 Presenting the mixed pixel problem in remotely sensed images (Tong et al., 2016).

The sub-pixel classification methods established are more appropriate, since the ratio of each land use mask category can be adjusted correctly (Lu & Weng, 2007). Sub-pixel classification techniques such as fuzzy, neural networks, regression modeling, regression tree evaluation, and spectral mixture evaluation were established in order to address the issue of mixed pixel. Therefore, several classification algorithms have been tested to map pondscapes in the study area and linear spectral unmixing, k-means unsupervised classification algorithms are selected to apply to develop pond detection algorithm. Flowchart of the process is presented in Figure 5.

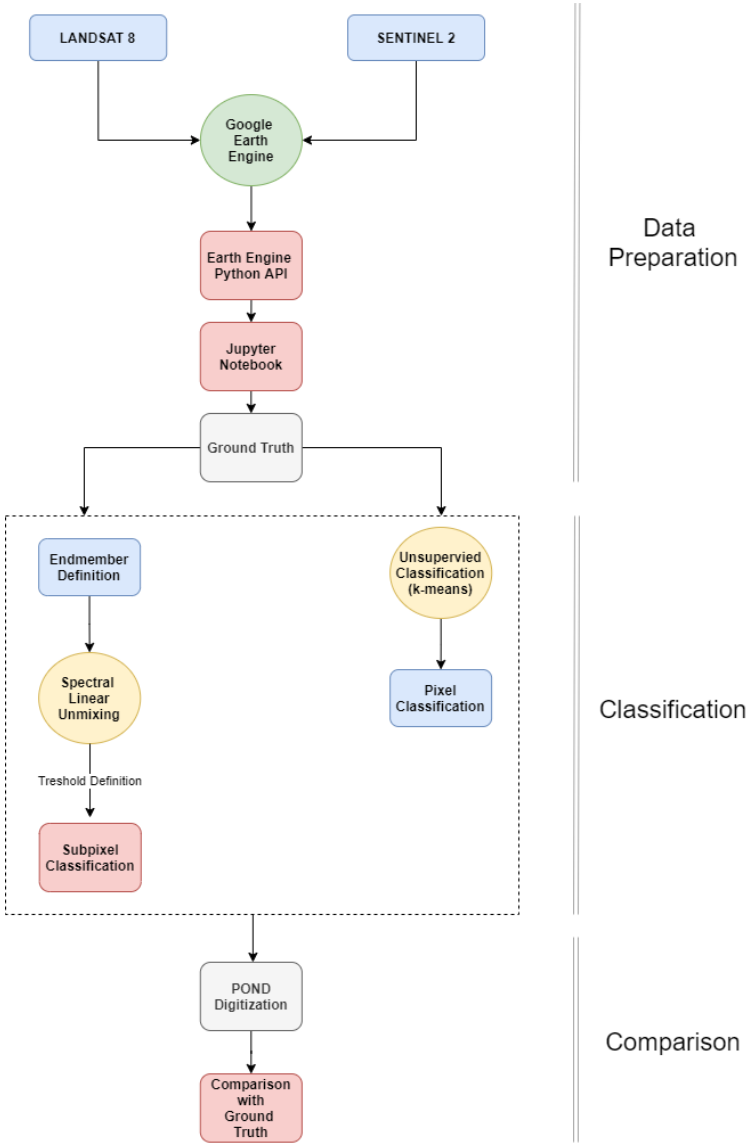


Figure 5 Flowchart of the developed application

Linear spectral unmixing algorithm performs subpixel classification and calculates the fractional abundance of different land cover types for individual pixels. However, spectral signatures of ground materials such as green vegetation, soil, or rock in the study area are needed to introduce as endmembers to a linear mixture model which can be inverted to compute endmember abundances for each data spectrum. Therefore, detailed analysis of land cover in the study area needed to be assessed in order to apply linear spectral unmixing. Since the local databases only have information about the location of the pondscape, it is not feasible to apply linear spectral mixing classification in all areas. Moreover, temporal changes in land cover in study area needs to be analyzed and endmembers should be updated in each image when investigating hydroperiods of pondscapes. As a result, K-means unsupervised classification algorithm have been applied to map pondscape considering it does not require human intervention and independent from the study area that is applied. In case of having snow in the scene, NDSI with an altitude threshold is used to differentiate the snow cover areas from water pixels.

# Results

4.1. Pre-processing of satellite data

Remote sensing images from Sentinel-2 images have been processed and used in mapping pondscapes in the study area due to their high temporal and spatial resolution. However, temporal coverage of Sentinel-2 is limited to 5 years. Landsat images will also be used where more temporal coverage is needed.

The Sentinel-2 mission has multi-spectral data with 13 bands in the visible, near infrared, and short-wave infrared part of the spectrum having spatial resolution of 10 m, 20 m and 60 m based on the bands (Table 1). High-resolution (10 m) RGB, Red Edge and lower resolution (20 m) NIR and SWIR bands are selected to be used in water detection algorithm.

Table 1. Sentinel-2 Band characteristics

| Sentinel-2 Bands | Central Wavelength (µm) | Resolution (m) |
|---|---|---|
| Band 1 - Coastal aerosol | 0.443 | 60 |
| Band 2 - Blue | 0.490 | 10 |
| Band 3 - Green | 0.560 | 10 |
| Band 4 - Red | 0.665 | 10 |
| Band 5 - Vegetation Red Edge | 0.705 | 20 |
| Band 6 - Vegetation Red Edge | 0.740 | 20 |
| Band 7 - Vegetation Red Edge | 0.783 | 20 |
| Band 8 - NIR | 0.842 | 10 |
| Band 8A - Vegetation Red Edge | 0.865 | 20 |
| Band 9 - Water vapour | 0.945 | 60 |
| Band 10 - SWIR - Cirrus | 1.375 | 60 |
| Band 11 - SWIR | 1.610 | 20 |
| Band 12 - SWIR | 2.190 | 20 |

First, Sentinel 2A images are filtered according to cloud coverage percentage to process cloudless images. Images having cloud coverage less than 20% have been selected. Then, clouds in the images are identified from the Sentinel cloud probability dataset (s2cloudless) and shadows are defined by cloud projection intersection with low-reflectance near-infrared (NIR) pixels. Identified clouds are masked so that images do not contain cloud interferences.

Pansharpening algorithm is applied to multispectral imagery to create a single high-resolution color image to match the spatial scale and to increase the image resolution. Pansharpening process merges the multispectral and panchromatic images, which gives the best of both image types, high spectral resolution, and medium spatial resolution (10 m) (Choi et al., 2019). This method is preferred since the area of the ponds in the study area (< *0.5 ha*) are not identifiable from raw satellite images, therefore spatial enhancement is needed. As an example, Figure 6 shows RGB Sentinel 2A image taken at 04/05/2020 in the Swiss study area. Figure 7 also shows original and pansharped images acquired on 04/05/2020.

Figure 6 RGB (Band 4, 3, 2) Sentinel 2A image acquired on 04/05/2020

Figure 7 False color (Bands 5,8A,12) Sentinel images (Original and pansharped images)

4.2. Processing of satellite data

RGB, Red Edge, NIR and SWIR bands (total of 8) are selected from pansharped multispectral Sentinel 2A images to produce the train dataset. Approximately 30000 train sets are produced from individual images belonging to a study area and 10 clusters are produced. Finally, clusters having water bodies are labelled as water body using the ponds from the ground truth. Figure 8 shows clustered image and labelled water bodies for the image acquired on 04/05/2020 for Switzerland study area.

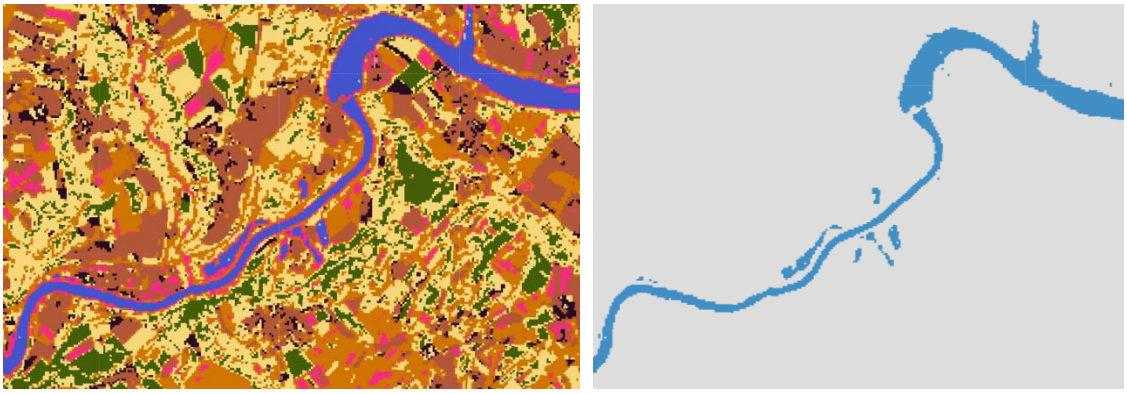

Figure 8 Clustered image and classified  water bodies

4.3. Testing the performance of the algorithm

Performance of the algorithm is assessed by comparing remotely sensed ponds with the ground truth data. Performance statistics for each pond are calculated by observing whether a pond is detected or not using the algorithm. The first validation study consists of 110 ponds, which has a surface area range 0.1– 4 ha. Sentinel 2A images according to the cloud coverage limitation are processed through 2017 to 2020. Hit or miss numbers of algorithm detecting the ponds in each image is calculated and yearly histograms are plotted accordingly. lectus massa, pharetra sit amet pharetra id, dictum quis felis. Cras convallis, arcu eget volutpat molestie, mi dui sollicitudin lorem, et tempus orci lacus ut velit.

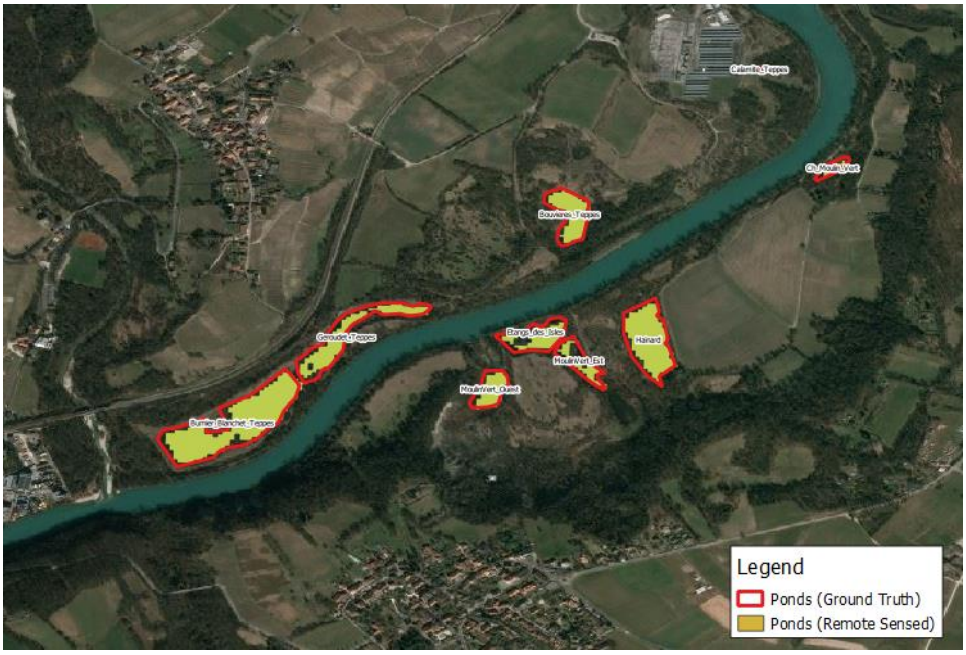


Figure 9 Remotely sensed ponds and ground truth

In addition, Figure 10 shows the number of found ponds in the Swiss study area in May for several years as a histogram. Month of May has been selected to display the performance of the algorithm since high water levels are observed in this month.

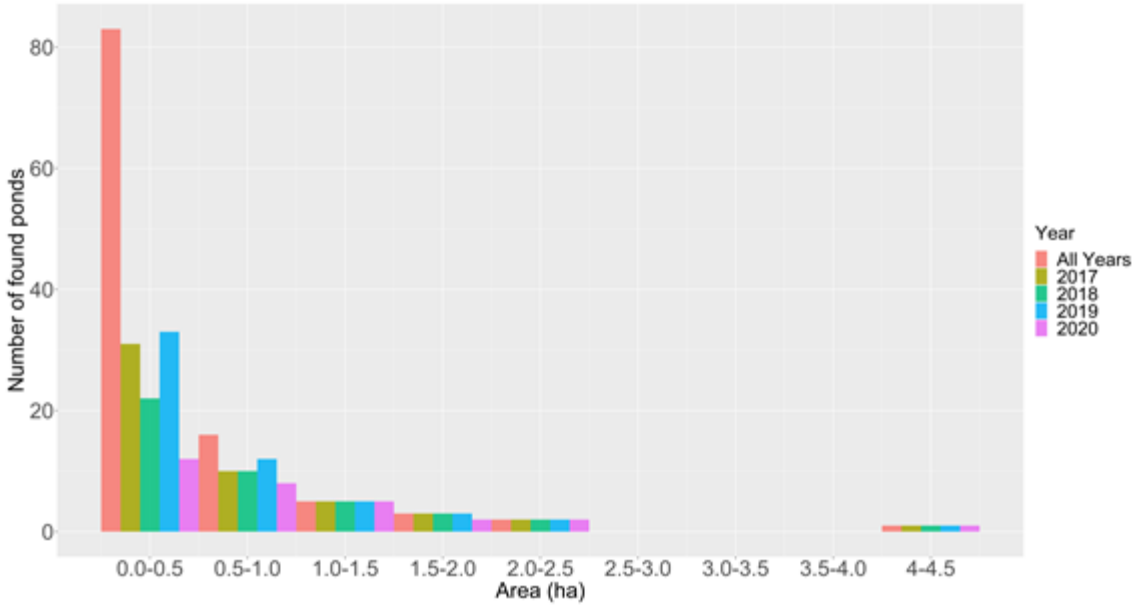


Figure 10 Number of found ponds retrieved from satellite images in May for four consecutive years in Switzerland

Figure 10 shows that ponds having surface area larger than 0.5 ha are successfully captured from satellite images by the classification algorithm. However, this figure only indicates the performance of the algorithm to map the ponds in the month of May. In order to monitor the hydroperiod of each pond, locally measured and remotely sensed surface areas are compared, and percentage of the area found from satellite images are calculated as in Eq. 1.

$$Area\ found\ ,\% = \frac{Remotely\ Sensed\ Area}{Localy\ Measured\ Area} * 100 \quad (1)$$

Figure 11 shows remotely monitored hydroperiod of pond '*Burnier Blanchet Teppes*', which has an area of 3.98 ha in Switzerland.

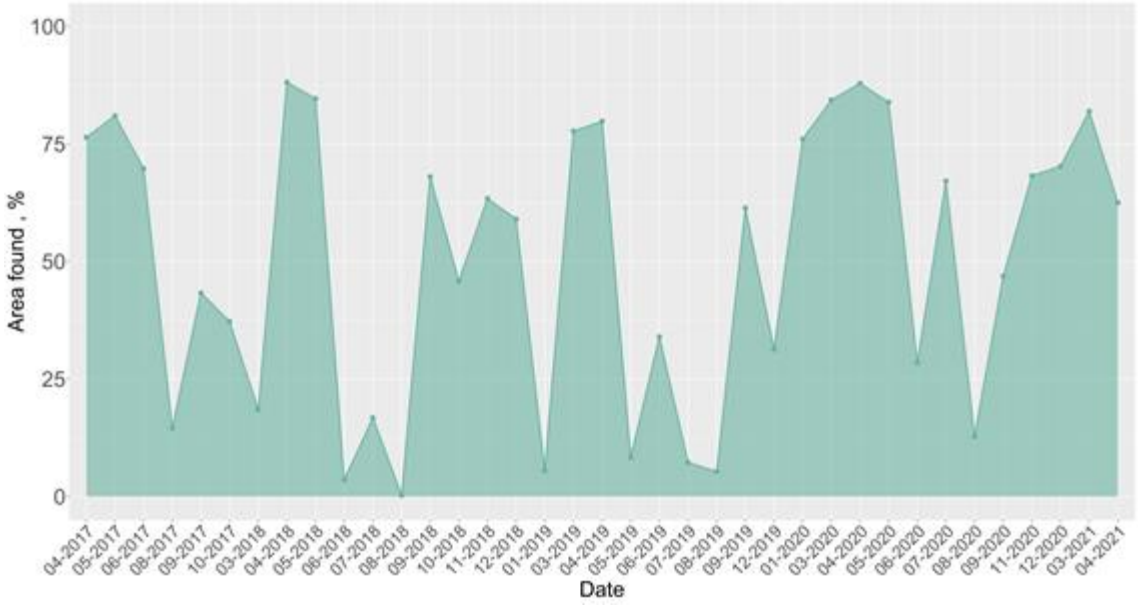


Figure 11 Monitored hydroperiod of 'Burnier Blanchet Teppes' pond

Sharp changes in area percentage and zero values of area percentage in Figure 11 might indicate that either ponds have been dried out or classification algorithm fails to identify ponds in the image. Therefore, further validation is needed using local observations.

# Conclusions

5.1. Improving the mapping accuracy

With the available medium size spatial resolution satellite data provides good performance for the ponds having surface area greater than 1 ha. In order to increase the mapping accuracy satellite data having high spatial data is needed to be used. WorldView-4 high resolution optical products are available as part of the DigitalGlobe Standard Satellite Imagery products from the QuickBird, WorldView-1/-2/-3/4, and GeoEye-1 satellites. In particular, WorldView-4 offers archive panchromatic products up to 0.31 m GSD resolution, and 4-Bands Multispectral products up to 1.24 m GSD resolution. The algorithm will be tested with high spatial data. Data are available for on demand ordering upon submission of a Project Proposal subject to evaluation and acceptance by ESA and the data owner. (https://earth.esa.int/eogateway/catalog/worldview-4-full-archive-and-tasking)

5.2. Final presentation of the ponds mapping and future dissemination

A web application has been developed to monitor hydroperiod of ponds in the study areas in Turkey, Switzerland, and Spain. The application allows users to visualize dynamically the ponds, and download measured and remotely sensed data (Figure 12). Web application can be accessed with following link:

https://ponderful.herokuapp.com

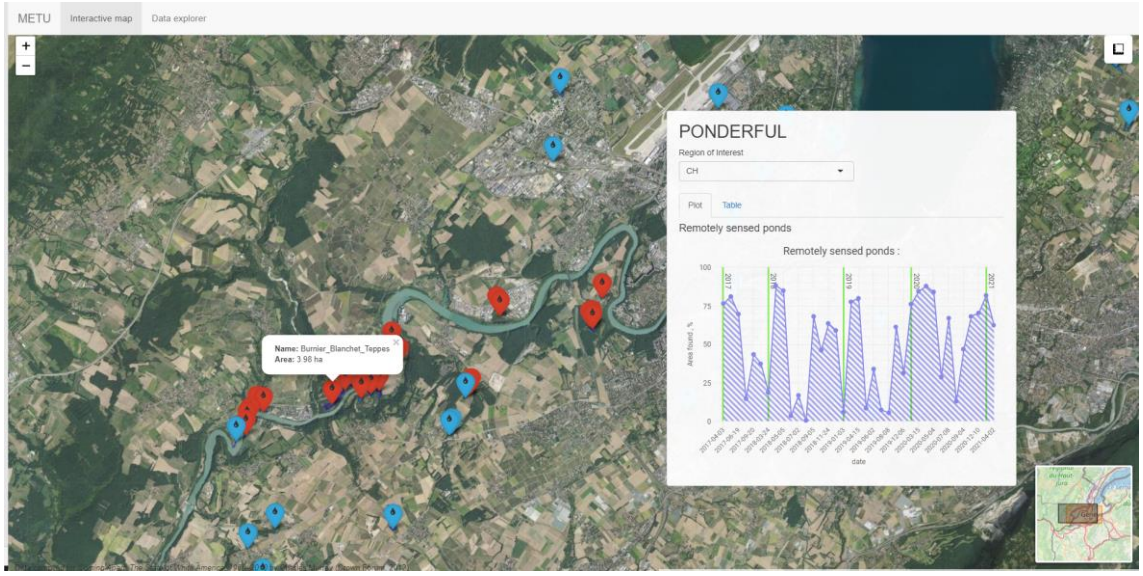


Figure 12: Developed web application to monitor hydroperiod of ponds

5.3. Planning 2021-2024

The algorithm for mapping the ponds will be tested with the ponds in the other countries contributing to PONDERFUL project, if needed it will be improved with new data.

WorldView-4 high resolution optical data will be obtained from ESA and the data will be used with the developed algorithm to map the ponds.

The hydroperiods of the ponds retrieved from satellite images will be compared with the water levels observed in the ponds from the stratified sampling and the DEMO-sites.

References


- Acharya, T. D., Lee, D. H., Yang, I. T., & Lee, J. K. (2016). Identification of water bodies in a Landsat 8 OLI image using a J48 Decision Tree. Sensors, 16(7), 1075.
- Chen, Y., Wang, B., Pollino, C. A., Cuddy, S. M., Merrin, L. E., & Huang, C. (2014). Estimate of flood inundation and retention on wetlands using remote sensing and GIS. Ecohydrology, 7, 1412–1420. https://doi.org/10.1002/eco.1467
- Choi, H., & Bindschadler, R. (2004). Cloud detection in Landsat imagery of ice sheets using shadow matching technique and automatic normalized difference snow index threshold value decision. Remote Sensing of Environment, 91(2), 237–242. https://doi.org/10.1016/j.rse.2004.03.007
- Choi, J., Park, H., & Seo, D. (2019). Pansharpening using guided filtering to improve the spatial clarity of VHR satellite imagery. *Remote Sensing*, *11*(6). https://doi.org/10.3390/rs11060633
- Chowdary, V. M., Chandran, R. V., Neeti, N., Bothale, R. V., Srivastava, Y. K., Ingle, P., et al. (2008). Assessment of surface and sub-surface waterlogged areas in irrigation command areas of Bihar state using remote sensing and GIS. Agricultural Water Management, 95(7),754–766. https://doi.org/10.1016/j.agwat.2008.02.009
- Frazier, P. S., & Page, K. J. (2000). Water body detection and delineation with Landsat TM data. Photogrammetric Engineering and Remote Sensing, 66(12), 1461–1467.
- Gebbinck, M. S. . (1998). Decomposition of Mixed Pixels in Remote Sensing Images to Improve the Area Estimation of Agricultural Fields (F. A. O. of the UN (ed.); p. 165). Katholieke Univ. Nijmegen.
- Huang, C., Chen, Y., Zhang, S., & Wu, J. (2018). Detecting, extracting, and monitoring surface water from space using optical sensors: A review. Reviews of Geophysics, 56, 333–360. https://doi.org/10.1029/2018RG000598
- Huang, C., Chen, Y., Wu, J., Li, L., & Liu, R. (2015). An evaluation of Suomi NPP-VIIRS data for surface water detection. Remote Sensing Letters, 6(2), 155–164. https://doi.org/10.1080/2150704X.2015.1017664

- Hui, F. M., Xu, B., Huang, H. B., Yu, Q., & Gong, P. (2008). Modelling spatial-temporal change of Poyang Lake using multitemporal Landsat imagery. International Journal of Remote Sensing, 29(20), 5767–5784. https://doi.org/10.1080/01431160802060912

- Lu, D., & Weng, Q. (2007). A survey of image classification methods and techniques for improving classification performance. In International Journal of Remote Sensing (Vol. 28, Issue 5). https://doi.org/10.1080/01431160600746456

- MacQueen, J. (1967). Some methods for classification and analysis of multivariate observations. Proceedings of the Fifth Berkeley Symposium on Mathematical Statistics and Probability, 1.

- Manavalan, P., Sathyanath, P., & Rajegowda, G. L. (1993). Digital image analysis techniques to estimate waterspread for capacity evaluations of reservoirs. Photogrammetric Engineering and Remote Sensing, 59(9), 1389–1395.

- McFeeters, S. K. (1996). The use of the normalized difference water index (NDWI) in the delineation of open water features. International Journal of Remote Sensing, 17(7), 1425–1432.

- Mohammadi, A., Costelloe, J. F., & Ryu, D. (2017). Application of time series of remotely sensed normalized difference water, vegetation and moisture indices in characterizing flood dynamics of large-scale arid zone floodplains. Remote Sensing of Environment, 190, 70–82. https:// doi.org/10.1016/j.rse.2016.12.003

- Olthof, I. (2017). Mapping seasonal inundation frequency (1985–2016) along the St-John River, New Brunswick, Canada using the Landsat archive. Remote Sensing, 9(2), 143.

- Ozesmi, S. L., & Bauer, M. E. (2002). Satellite remote sensing of wetlands. Wetlands Ecology and Management, 10(5), 381–402. https://doi.org/10.1023/a:1020908432489

- Richards, J. A. (2013). Remote sensing digital image analysis: An introduction. In Remote Sensing Digital Image Analysis: An Introduction (Vol. 9783642300622). https://doi.org/10.1007/978-3-642-30062-2

- Salomonson, V. V., & Appel, I. (2004). Estimating fractional snow cover from MODIS using the normalized difference snow index. Remote Sensing of Environment, 89(3), 351–360. https://doi.org/10.1016/j.rse.2003.10.016

- Sun, D. L., Yu, Y. Y., & Goldberg, M. D. (2011). Deriving water fraction and flood maps from MODIS images using a decision tree approach. IEEE Journal of Selected Topics Applied Earth Observation Remote Sensing, 4(4), 814–825. https://doi.org/10.1109/jstars.2011.2125778

- Tong L., Zhaou, J., Qian, Y., Bai, X., & Gao, Y. (2016). Nonnegative matrix factorization based hyperspectral unmixing with partially known endmembers. IEEE Transactions on Geoscience and Remote Sensing , 54(11), 6531-6544.

- Topp S.N., Pavesky, T.M., Jensen, D., & Ross, M.R. (2020). Research Trends in th euse of remote sensing for inland quality science: Moving towards multidiciplinary applications. Water, 12, 169; https://doi:10.3390/w12010169

- Tso, B., & Mather, P. M. (2010). Pattern recognition principles. In Classification Methods for Remotely Sensed Data. https://doi.org/10.4324/9780203303566_chapter_2

- Xu, H. Q. (2006). Modification of normalised difference water index (NDWI) to enhance open water features in remotely sensed imagery. International Journal of Remote Sensing, 27(14), 3025–3033.

Appendix:

Table A1: Pond database of Switzerland

| id | Date | Name | Surface | Depth_max | Depth_mean | L_bank | Altitude | Area |
|---|---|---|---|---|---|---|---|---|
| 1 | 4/3/2017 | Mouilles | 3000 | 310 | 126 | 577 | 414 | 0.94 |
| 2 | 4/3/2017 | Combes-Chapuis | 3340 | 120 | 70 | 614 | 462 | 0.52 |
| 3 | 4/3/2017 | Laconnex | 2600 | 250 | 194 | 283 | 433 | 0.55 |
| 4 | 4/3/2017 | Bois-Vieux | 3582 | 140 | 80 | 357 | 493 | 0.38 |
| 5 | 4/3/2017 | Feuillets | 1062 | 150 | 100 |  | 490 | 0.11 |
| 6 | 4/3/2017 | Pre-Bordon_aval | 1070 | 100 | 57 | 107 | 469 | 0.06 |
| 7 | 4/3/2017 | Pre-Bordon_amont | 790 | 95 | 85 | 96 | 469 | 0.04 |
| 8 | 4/3/2017 | Dolliets | 2980 | 136 | 90 | 434 | 486 | 0.18 |
| 9 | 4/3/2017 | Arales_aval | 790 | 220 | 100 | 146 | 494 | 0.02 |
| 10 | 4/3/2017 | Arales_amont | 550 | 100 | 66 | 85 | 496 | 0.01 |
| 11 | 4/3/2017 | Rapes | 1410 | 110 | 80 | 241 | 466 | 0.11 |
| 12 | 4/3/2017 | Prejins | 142 | 100 | 48.3 | 50 | 428 | 0.01 |
| 13 | 4/3/2017 | BIT | 3754 | 23 | 18.5 | 300 | 443 | 0.43 |
| 14 | 4/3/2017 | Loex-Hopital | 500 | 73 | 66.9 | 82 | 409 | 0.05 |
| 15 | 4/3/2017 | Franchises | 224 | 60 | 40 | 71 | 419 | 0.15 |
| 16 | 4/3/2017 | Paix | 263 | 21 | 20.5 | 114 | 426 | 0.02 |
| 17 | 4/3/2017 | Vessy | 500 | 100 | 58 | 122 | 414 | 0.01 |
| 18 | 4/3/2017 | Parc_Bertrand | 275 | 42 | 39.1 | 88 | 417 | 0.03 |
| 19 | 4/3/2017 | Zulian | 439 | 90 | 63.7 | 76 | 418 | 0.04 |
| 20 | 4/3/2017 | Cimetiere_St_Georges | 675 | 79 | 65.9 | 149 | 420 | 0.07 |
| 21 | 4/3/2017 | Jardin_botanique | 560 | 88 | 75.3 | 140 | 382 | 0.06 |
| 22 | 4/3/2017 | Jardin_bota2_serres | 120 | 54 | 52 | 50 | 389 | 0.01 |
| 23 | 4/3/2017 | BoisdeBay_calamite | 42 | 30 | 25 | 15 | 376 | 0.01 |
| 24 | 4/3/2017 | BoisdeBay_ancien | 90 | 13 | 8.4 | 45 | 375 | 0.01 |
| 25 | 4/3/2017 | BoisdeBay_recolte_toit | 140 | 42 | 29.7 | 55 | 375 | 0.01 |

Table A:2 Pond database of Spain

| id | date | Name | ALT | PRE | TMIT | TMIN | TMAX | ORI | Area |
|---|---|---|---|---|---|---|---|---|---|
| 1 | 4/3/2017 | Bassa de Ponent | 139 | 641 | 15.7 | -4.8 | 37 | Natural | 0.20 |
| 2 | 4/3/2017 | Estany de la Rajoleria de la Gutina | 152 | 641 | 15.7 | -4.8 | 37 | Natural | 0.08 |
| 3 | 4/3/2017 | Bassa dels Torlits | 142 | 641 | 15.7 | -4.8 | 37 | Natural | 1.74 |
| 4 | 4/3/2017 | Estanyol de la Cardonera de la Gutina | 152 | 641 | 15.7 | -4.8 | 37 | Natural | 0.20 |
| 5 | 4/3/2017 | Bassa del Mas Faig | 133 | 641 | 15.7 | -4.8 | 37 | Natural | 0.43 |
| 6 | 4/3/2017 | Bassa del Serrat de les Garrigues | 144 | 641 | 15.7 | -4.8 | 37 | Natural | 0.03 |
| 7 | 4/3/2017 | Estany Petit dels Torlits | 142 | 641 | 15.7 | -4.8 | 37 | Natural | 0.87 |
| 8 | 4/3/2017 | Estany de les Moles | 139 | 641 | 15.7 | -4.8 | 37 | Natural | 0.47 |
| 9 | 4/3/2017 | Prat del Serrat de les Garrigues | 143 | 641 | 15.7 | -4.8 | 37 | Natural | 0.51 |
| 10 | 4/3/2017 | Estany Gran de Canadal | 171 | 641 | 15.7 | -4.8 | 37 | Natural | 0.00 |
| 11 | 4/3/2017 | Bassa de Llevant | 145 | 641 | 15.7 | -4.8 | 37 | Natural | 0.26 |
| 12 | 6/2/2017 | Bassa de Ponent | 139 | 641 | 15.7 | -4.8 | 37 | Natural | 0.20 |
| 13 | 6/2/2017 | Estany de la Rajoleria de la Gutina | 152 | 641 | 15.7 | -4.8 | 37 | Natural | 0.08 |
| 14 | 6/2/2017 | Bassa dels Torlits | 142 | 641 | 15.7 | -4.8 | 37 | Natural | 1.74 |
| 15 | 6/2/2017 | Estanyol de la Cardonera de la Gutina | 152 | 641 | 15.7 | -4.8 | 37 | Natural | 0.20 |
| 16 | 6/2/2017 | Bassa del Mas Faig | 133 | 641 | 15.7 | -4.8 | 37 | Natural | 0.43 |
| 17 | 6/2/2017 | Bassa del Serrat de les Garrigues | 144 | 641 | 15.7 | -4.8 | 37 | Natural | 0.03 |
| 18 | 6/2/2017 | Estany Petit dels Torlits | 142 | 641 | 15.7 | -4.8 | 37 | Natural | 0.87 |
| 19 | 6/2/2017 | Estany de les Moles | 139 | 641 | 15.7 | -4.8 | 37 | Natural | 0.47 |
| 20 | 6/2/2017 | Prat del Serrat de les Garrigues | 143 | 641 | 15.7 | -4.8 | 37 | Natural | 0.51 |
| 21 | 6/2/2017 | Estany Gran de Canadal | 171 | 641 | 15.7 | -4.8 | 37 | Natural | 0.00 |
| 22 | 6/2/2017 | Bassa de Llevant | 145 | 641 | 15.7 | -4.8 | 37 | Natural | 0.26 |
| 23 | 7/2/2017 | Bassa de Ponent | 139 | 641 | 15.7 | -4.8 | 37 | Natural | 0.20 |
| 24 | 7/2/2017 | Estany de la Rajoleria de la Gutina | 152 | 641 | 15.7 | -4.8 | 37 | Natural | 0.08 |
| 25 | 7/2/2017 | Bassa dels Torlits | 142 | 641 | 15.7 | -4.8 | 37 | Natural | 1.74 |

# Ponderful

**Coordinator**: Prof. Sandra Brucet, University of Vic – Central University of Catalonia

**Project Manager**: Dr. Diana van Gent, University of Vic – Central University of Catalonia

**Contact**: diana.vangent@uvic.cat

**Duration:** 1 December 2020 to 1 December 2024

**Website:** www.ponderful.eu

**Facebook:** /Ponderful-331847228188664

**Twitter**: @ponds4climate

**Pond Ecosystems for Resilient Future Landscapes in a Changing Climate**

This project has received funding from the European Union's Horizon 2020 Research and Innovation Programme under Grant Agreement No ID 869296